Electronic Supplementary Material (ESI) for ChemComm.

Fluorene-fused Dimeric Carbonyl/amine Multiresonant Thermally Activated Delayed Fluorescence Emitter for Efficient Green OLEDs

Sen Wu,[a] *Ya-Nan Hu,*[b] *Dianming Sun,*[a*] *Kai Wang,*[b] *Xiao-Hong Zhang*[b,c*] and *Eli Zysman-Colman*[a*]

[a]Organic Semiconductor Centre, EaStCHEM School of Chemistry, University of St Andrews, St Andrews, Fife, UK, KY16 9ST, Fax: +44-1334 463808; Tel: +44-1334 463826; E-mail: eli.zysman-colman@st-andrews.ac.uk; sd235@st-andrews.ac.uk.

[b]Institute of Functional Nano & Soft Materials (FUNSOM), Joint International Research Laboratory of Carbon-Based Functional Materials and Devices, Soochow University, Suzhou, Jiangsu 215123, P. R. China. E-mail: xiaohong_zhang@suda.edu.cn.

[c]Jiangsu Key Laboratory of Advanced Negative Carbon Technologies, Soochow University, Suzhou, 215123, Jiangsu, P. R. China

Table of Contents

General methods

General Synthetic Procedures. The other reagents and solvents were obtained from commercial sources and used as received unless otherwise stated. Air-sensitive reactions were done under a nitrogen atmosphere using Schlenk techniques. Dry solvents used in the reaction were obtained from a MBRAUN SPS5 solvent purification system. Flash column chromatography was carried out using silica gel (Silia-P from Silicycle, 60 Å, 40-63 μm). Analytical thin-layer-chromatography (TLC) was performed with silica plates with aluminium backings (250 μm with F-254 indicator). TLC visualization was accomplished by 254/365 nm UV lamp. HPLC was conducted on a Shimadzu LC-40 HPLC system. HPLC traces were performed using a Shim-pack GIST 3μm C18 reverse phase analytical column. ^{1}H and ^{13}C and NMR spectra were recorded on a Bruker Advance spectrometer (400 MHz for ^{1}H and 126 MHz for ^{13}C). The following abbreviations have been used for multiplicity assignments: "s" for singlet, "d" for doublet, "t" for triplet, "m" for multiplet, "dd" for doublet of doublets, "dt" for doublet of triplets. ^{1}H and ^{13}C NMR spectra were referenced to the solvent peaks). Melting points were measured using open-ended capillaries on an Electrothermal 1101D Mel-Temp apparatus and are uncorrected. High-resolution mass spectrometry (HRMS) was performed at University of Edinburgh Mass Spectrometry Facility. Elemental analyses were performed by Dr. Joe Casillo at the University of Edinburgh.

Quantum chemical calculations. The calculations were performed using Density Functional Theory (DFT) within Gaussian 16[1] as well as the second order algebraic diagrammatic construction Spin-Component Scaling (ADC(2)-SCS)[2] method using the Turbomole/7.5 package.[3] For the DFT calculations, the ground-state and excited singlet state were optimized using the PBE0[4] functional and the 6-31G(d,p) basis set,[5] and the excited-state calculations were performed using Time-Dependent DFT within the Tamm-Dancoff approximation (TDA-DFT)[4,6] with the same functional and basis set as for the ground-state geometry optimization in the gas phase. Spin-orbit coupling matrix elements SOCME were calculated based on the optimized excited triplet-state geometry. Spin-orbit coupling matrix elements between singlet and triplet excited states were calculated using the PySOC program.[7] The molecular orbital distributions were visualized with Gaussview 5.0[8] and using Silico 1.0, an in-house built software package.[9–11] For the ADC(2) calculations, the ground states was optimized using the ADC(2)-SCS functional and the cc-pVDZ basis set in the gas phase based on the geometry calculated by DFT.[2] Vertical transitions to the excited states were performed based on the ground-state optimized structure. Difference density plots were used to visualize change in electronic density between the ground and excited state and were visualized using the VESTA package.[12] The RMSD of ground state and excited singlet state was visualized using VMD

program.[13] Simulated emission spectra were obtained by Franck-Condon analysis of the S_1-S_0 transition under vacuum based on B3LYP/6-31G(d,p).[14,15]

Electrochemistry measurements. Cyclic Voltammetry (CV) analysis was performed on an Electrochemical Analyzer potentiostat model 620E from CH Instruments at a sweep rate of 100 mV/s. Differential pulse voltammetry (DPV) was conducted with an increment potential of 0.004 V and a pulse amplitude, width, and period of 50 mV, 0.05, and 0.5 s, respectively. Samples were prepared in DCM solutions, which were degassed by sparging with DCM-saturated nitrogen gas for 5 minutes prior to measurements. All measurements were performed using 0.1 M DCM solution of tetra-*n*-butylammonium hexafluorophosphate, [^{n}Bu$_4$N]PF$_6$. An Ag/Ag$^+$ electrode was used as the reference electrode while a platinum electrode and a platinum wire were used as the working electrode and counter electrode, respectively. The redox potentials are reported relative to a saturated calomel electrode (SCE) with a ferrocenium/ferrocene (Fc/Fc$^+$) redox couple as the internal standard (0.46 V vs SCE).[16] The HOMO and LUMO energies were determined using the relation $E_{HOMO/LUMO} = -(E_{ox} / E_{red} + 4.8)$ eV, where E_{ox} and E_{red} are the onset of anodic and cathodic peak potentials, respectively calculated from DPV relative to Fc/Fc$^+$.[17]

Photophysical measurements. Optically dilute solutions of concentrations on the order of 10^{-5} or 10^{-6} M were prepared in spectroscopic grade solvents for absorption and emission analysis. Absorption spectra were recorded at room temperature on a Shimadzu UV-2600 double beam spectrophotometer with a 1 cm quartz cuvette. Molar absorptivity determination was verified by linear regression analysis of values obtained from at least four independent solutions at varying concentrations ranging from 3.0×10^{-6} to 1.0×10^{-5} with absorbance ranging from 0.025 to 0.100. For emission studies, steady-state emission and time-resolved emission spectra were recorded at room temperature using an Edinburgh Instruments FS5 fluorimeter. Samples were excited at 340 nm for steady-state measurements and 379 nm for time-resolved PL decays. Photoluminescence quantum yields for solutions were determined using the optically dilute method, in which four sample solutions with absorbances of ca. 0.10, 0.075, 0.050 and 0.025 at 360 nm were used.[18] The Beer-Lambert law was found to remain linear at the concentrations of the solutions. For each sample, linearity between absorption and emission intensity was verified through linear regression analysis with the Pearson regression factor (R^2) for the linear fit of the data set surpassing 0.9. Individual relative quantum yield values were calculated for each solution and the values reported represent the slope obtained from the linear fit of these results. The quantum yield of the sample, Φ_{PL}, was determined using the equation $\Phi_{PL} = (\Phi_r * \frac{A_r}{A_s} * \frac{I_s}{I_r} * \frac{n_s^2}{n_r^2})$,[18] where A stands for the absorbance at the excitation wavelength (λ_{exc} = 340 nm), I is the integrated area under the corrected emission curve and n is the refractive index of the

solvent with the subscripts "s" and "r" representing sample and reference respectively. Φ_r is the absolute quantum yield of the external reference quinine sulfate (Φ_r = 54.6% in 1 *N* H_2SO_4).[19]

An integrating sphere (Edinburgh Instruments FS5, SC30 module) was employed for the photoluminescence quantum yield measurements of the thin film samples. The Φ_{PL} of the films were then measured in air and in N_2 by purging the integrating sphere with N_2 gas flow for 2 min. The photophysical properties of the film samples were measured using an Edinburgh Instruments FS5 fluorimeter. Time-resolved PL measurements of the thin films were carried out using the multi-channel scaling (MCS) and time-correlated single-photon counting (TCSPC) technique. The samples were excited at 379 nm by a pulsed laser and were kept in a vacuum of $< 8 \times 10^{-4}$ mbar. The singlet and triplet state energies in 2-MeTHF glass and in doped film were determined from the onset values of the steady-state photoluminescence PL (SSPL) and phosphorescence spectra at 77 K. The singlet-triplet energy gap (ΔE_{ST}) was estimated from the difference in energy of the steady-state PL and phosphorescence spectra. The samples were excited by a xenon flashlamp emitting at 340 nm (EI FS5, SC-70). Phosphorescence spectra were measured with a time-gated window of 1-10 ms.

Fitting of time-resolved luminescence measurements: Time-resolved PL measurements were fitted to a sum of exponentials decay model, with chi-squared (χ^2) values between 1 and 2, using the EI FS5 Each component of the decay is assigned with a weight, (w_i), which is the contribution of the emission from each component to the total emission.

The average lifetime was then calculated using the following expressions:

1. Two exponential decay model:

$$\tau_{AVG} = \tau_1 w_1 + \tau_2 w_2 \qquad \text{(S1)}$$

with weights defined as $w_1 = \frac{A1\tau_1}{A1\tau_1 + A2\tau_2}$ and $w_2 = \frac{A2\tau_2}{A1\tau_1 + A2\tau_2}$ where A_1 and A_2 are the preexponential-factors of each component.

2. Three exponential decay model:

$$\tau_{AVG} = \tau_1 w_1 + \tau_2 w_2 + \tau_3 w_3 \qquad \text{(S2)}$$

with weights defined as $w_1 = \frac{A1\tau_1}{A1\tau_1 + A2\tau_2 + A3\tau_3}$, $w_2 = \frac{A2\tau_2}{A1\tau_1 + A2\tau_2 + A3\tau_3}$ and $w_3 = \frac{A3\tau_3}{A1\tau_1 + A2\tau_2 + A3\tau_3}$ where A_1, A_2 and A_3 are the preexponential-factors of each component.

OLED Fabrication and Characterization: The OLED devices were fabricated in a bottom-emitting structure via thermal evaporation in a high vacuum at a base pressure of $<5\times10^{-7}$ mbar.

A pre-patterned glass substrate coated with indium doped tin oxide (ITO) was cleaned sequentially by ultrasonication in acetone, and isopropanol for 15 minutes. The temperature of ultrasonication bath was set at 60-70 ºC. The cleaned substrate was exposed to oxygen plasma for 3 min to remove all dust and organics on the ITO surface and to increase the work function of ITO anode for better hole injection from the anode to organic layer. The substrate was loaded in the thermal evaporator. Organic layers were deposited at a rate of 0.3-1.0 Å/s, monitored using a quartz crystal. The electron injection layer, LiF, was deposited at a rate of 0.05 Å/s, while the Al cathode was deposited initially with a rate of 0.5 Å/s to obtain 10 nm thickness and after that the rate of Al cathode was increased to 3 Å/s. Two custom-made shadow masks were used to define the area of the evaporations. The organic layers and LiF were evaporated with a same shadow mask, but Al were evaporated with the other mask. The active area of the OLED was 2 mm^2, determined by the spatial overlap of the anode and cathode electrodes. All the devices were encapsulated with glass lids and UV epoxy resin inside a N_2 filled globe box. The luminance-current-voltage characteristics were measured in an ambient environment using a Keithley 2400 source meter and a homemade photodiode circuit connected to a Keithley 2000 multimeter for the voltage reading. The external quantum efficiency was calculated assuming Lambertian emission pattern for the OLEDs. The electroluminescence spectra were recorded by an Andor DV420-BV CCD spectrometer.

Experimental section

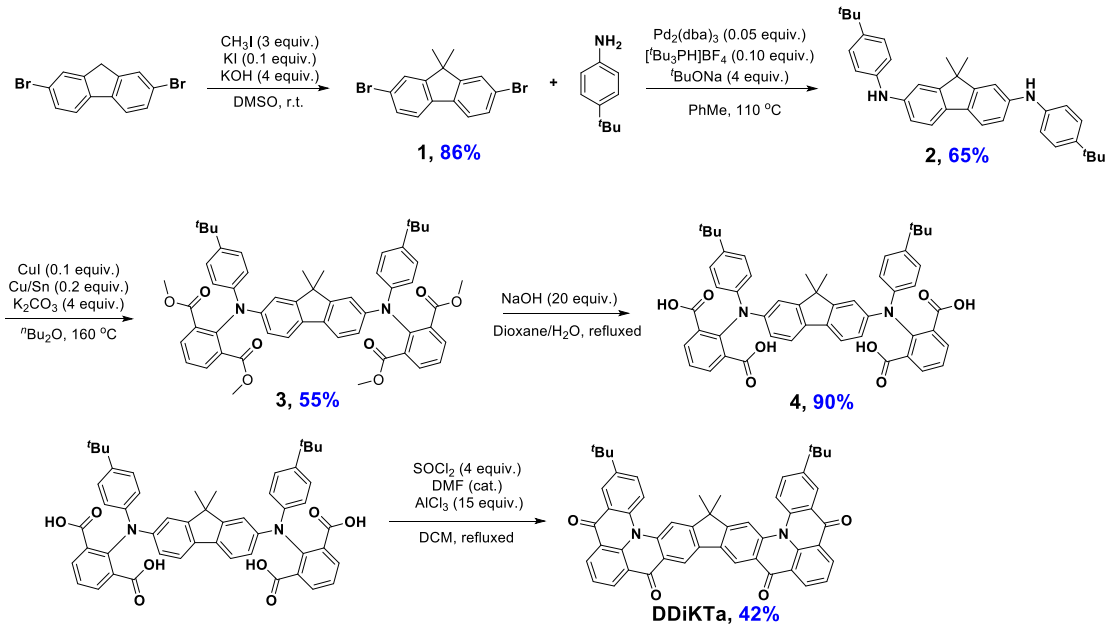

Scheme **S1**. Synthesis route of **DDiKTa-F**.

2,7-dibromo-9,9-dimethyl-fluorene (1)

2,7-dibromo-fluorene (15.00 g, 46.29 mmol, 1.0 equiv.), potassium hydroxide (10.39 g, 185.2 mmol, 4.0 equiv.) and a catalytic amount of potassium iodide (0.77 g, 4.63 mmol, 0.1 equiv.) were stirred in dimethylsulfoxide (80 mL). Iodomethane (19.71 g, 138.90 mmol, 3.0 equiv.) was added dropwise slowly. The reaction was stirred at room temperature for 24 and then poured into 500 mL of water. The product was extracted with dichloromethane (DCM) (2×250 mL) and the combined organic layers were evaporated to dryness. The crude product was purified by flash column chromatography on silica gel (DCM: Hexane = 1:5) to afford a white solid. **Yield**: 86% (14 g). **R_f:** 0.3 (DCM: Hexane = 1:5). **Mp**: 177-179 ℃. ^{1}H NMR (400 MHz, $CDCl_3$): δ 7.59 – 7.54 (m, 4H), 7.49 (dd, J = 8.1, 1.7 Hz, 2H), 1.49 (s, 6H). The compound characterization matches that previously reported.[20]

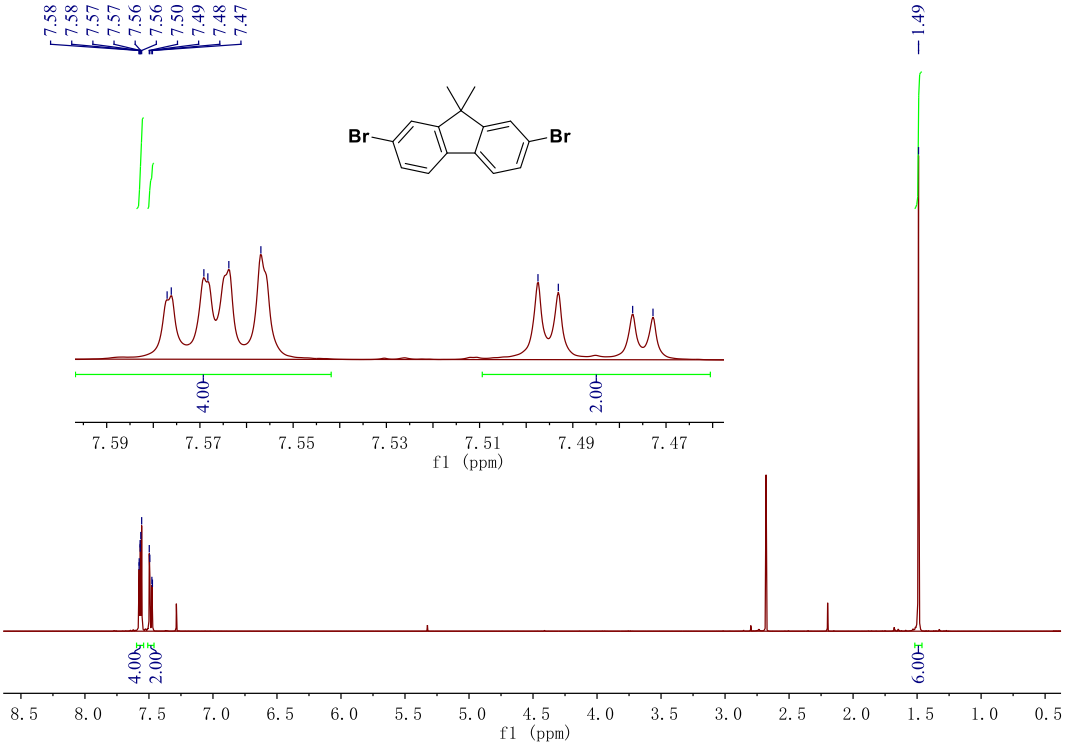

Figure **S1**. ^{1}H NMR spectrum of **1** in $CDCl_3$.

N_2,N_7-bis(4-(tert-butyl)phenyl)-9,9-dimethyl-9H-fluorene-2,7-diamine (2)

Compound **1** (5.00 g, 14.2 mmol, 1.0 equiv.), 4-(*tert*-butyl)aniline (12.7 g, 85.2 mmol, 6.0 equiv.), sodium *tert*-butoxide (6.83, 85.2 mmol, 6.0 equiv.), $Pd_2(dba)_3$ (0.39 g, 0.43 mmol, 0.03 equiv.) and [$^{t}Bu_3PH$]BF_4 (0.25 g, 0.85 mmol, 0.06 equiv.) were added to a Schlenk flask containing 100 mL of anhydrous toluene. After degassing the flask, the reaction system was placed under a nitrogen atmosphere. The mixture was heated at 115 °C for 24 h. After cooling to room temperature, DCM (200 mL) was added to the mixture. The mixture was washed with a saturated NaCl aqueous solution (2× 200 mL). The collected organic phase was dried over anhydrous sodium sulfate and concentrated under reduced pressure. The collected crude product was purified by silica gel column chromatography (EtOAc: hexane = 1:10, $\mathbf{R_f}$: 0.35) to afford the target compounds with white powder. **Yield**. 4.5 g, 65%. **R_f:** 0.4 (DCM: Hexane = 1:2). **Mp**: 201-203 °C. **^{1}H NMR (400 MHz, DMSO):** δ 8.09 (s, 2H), 7.49 (d, J = 8.1 Hz, 2H), 7.27 (d, J = 8.6 Hz, 4H), 7.14 (d, J = 1.9 Hz, 2H), 7.06 – 7.01 (m, 4H), 6.98 (dd, J = 8.2, 2.0 Hz, 2H), 1.39 (s, 6H), 1.27 (s, 18H). **^{13}C NMR (101 MHz, DMSO)** δ 154.45, 142.62, 142.14, 141.58, 131.41, 126.25, 119.95, 116.86, 115.78, 111.51, 46.57, 34.25, 31.84, 27.82. **HRMS [M^+]**: Calculated: 488.3186 ($C_{35}H_{40}N_2$); Found: 488.3202.

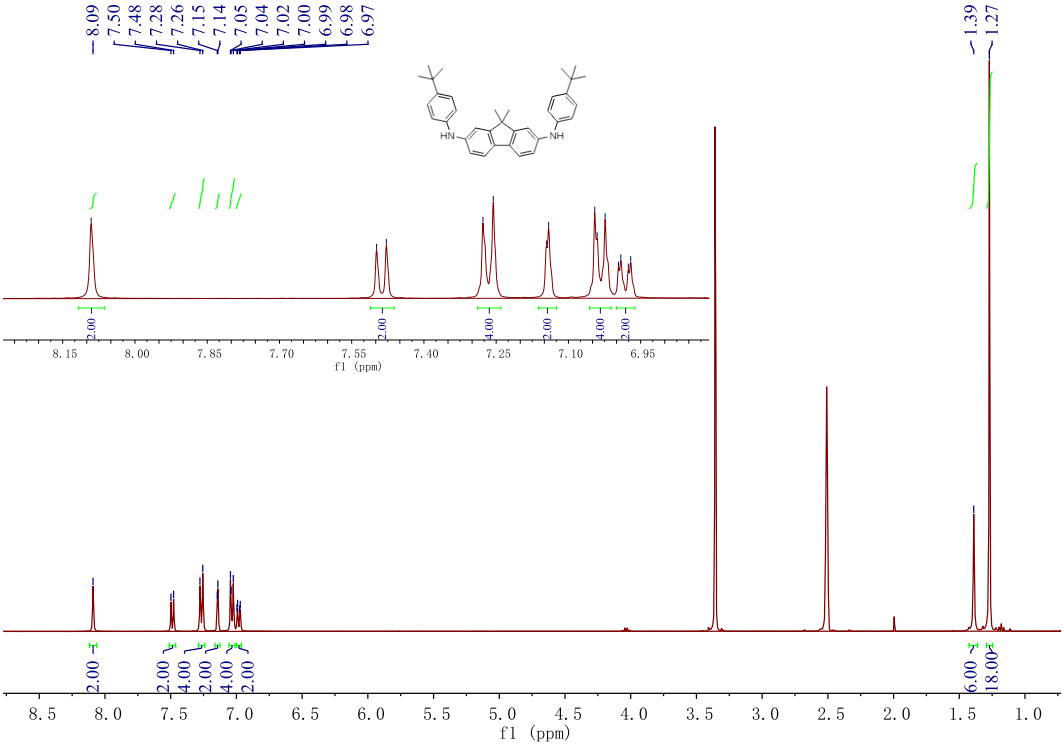

Figure **S2**. [1]H NMR spectrum of **2** in DMSO.

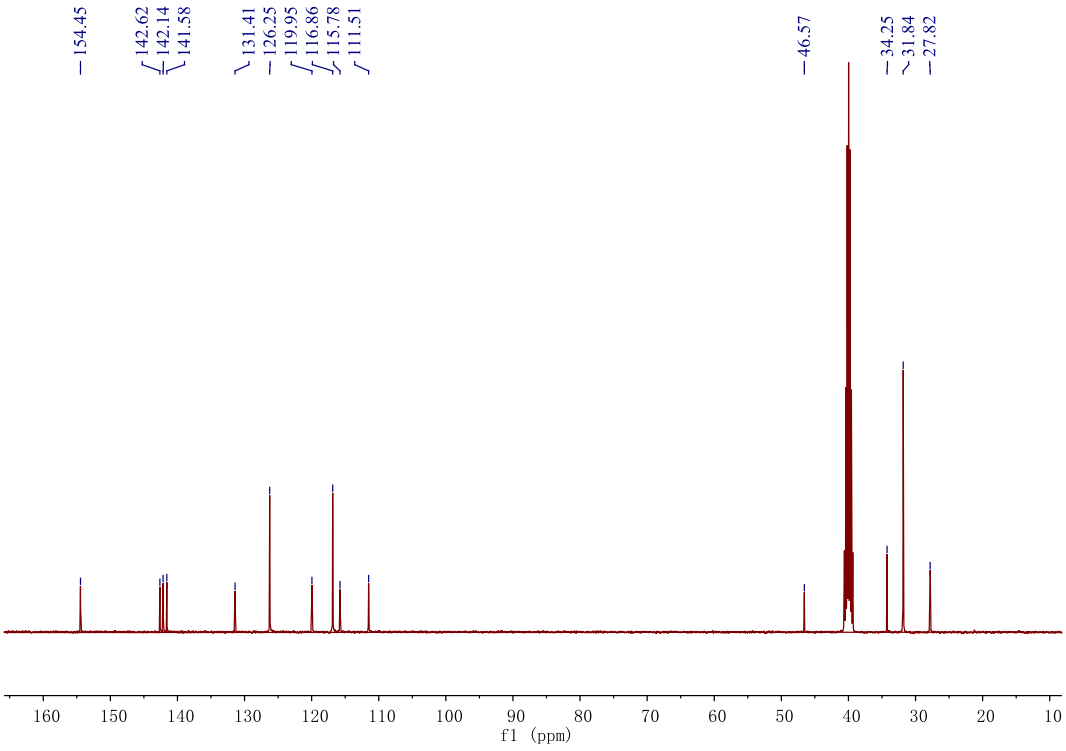

Figure **S3**. [13]C NMR spectrum of **2** in DMSO.

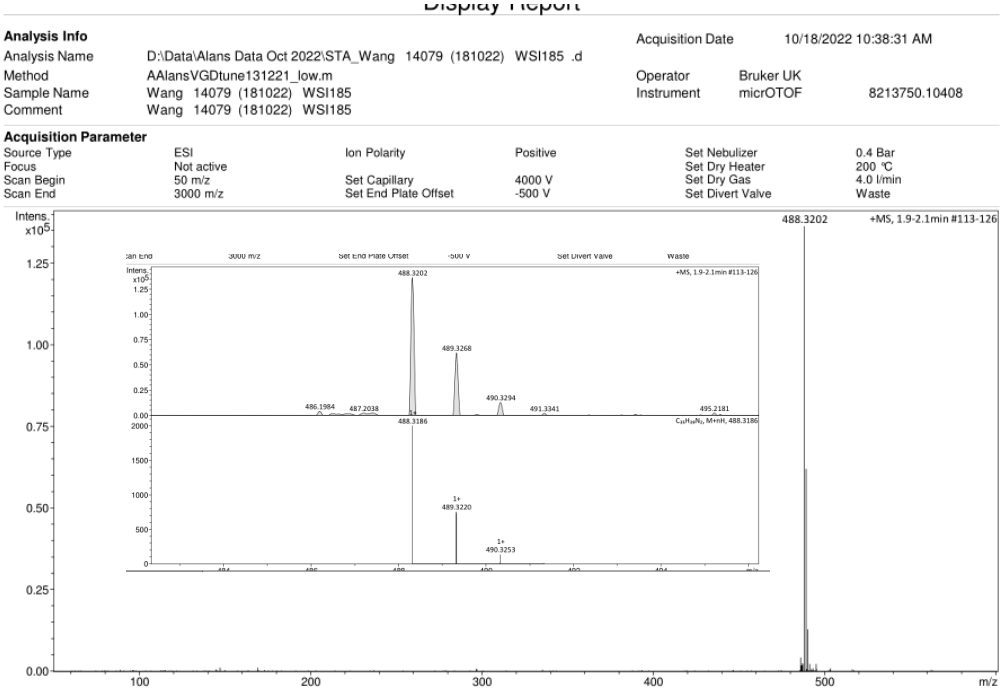

Figure **S4**. HRMS spectrum of **2.**

2,2'-((9,9-dimethyl-9H-fluorene-2,7-diyl)bis((4-(tert-butyl)phenyl)azanediyl))diisophthalic acid (4)

2 (2.50 g, 5.12 mmol, 1.0 equiv.), 2-bromoisophthalic acid dimethyl ester (4.19 g, 15.3 mmol, 3.0 equiv.), potassium carbonate (4,24 g, 30.7 mmol, 6.0 equiv.), CuI (0.10 g, 0.51 mmol, 0.1 equiv.), Cu/Sn (0.10 g, 0.51 mmol, 0.1 equiv.) and 2,2,6,6-tetramethyl-3,5-heptanedione ((^{t}BuCO)$_2$CH$_2$, 0.09 g, 0.51 mmol, 0.1 equiv.) were added to a Schlenk flask containing 40 mL of anhydrous dibutyl ether. After degassing the flask, the reaction system was placed under a nitrogen atmosphere. The mixture was heated at 145 °C for 3 days. After cooling to room temperature, DCM (50 mL) was added to the mixture. The mixture was washed with a saturated NaCl aqueous solution (3 × 50 mL). The collected organic phase was dried over anhydrous sodium sulfate and concentrated under reduced pressure. The collected crude product was purified by silica gel column chromatography (EtOAc:hexane = 1:5, **R$_f$**: 0.30) to afford the target compounds **3** with dark yellow powder. **Yield**. 3.7 g, 83%. **^{1}H NMR (400 MHz, DMSO)** δ 7.75 (d, J = 7.7 Hz, 4H), 7.49 (d, J = 8.2 Hz, 2H), 7.42 (s, 2H), 7.25 (d, J = 8.8 Hz, 4H), 6.98 (d, J = 2.1 Hz, 2H), 6.83 – 6.78 (m, 4H), 6.70 (dd, J = 8.2, 2.1 Hz, 2H), 3.35 (s, 12H), 1.26 (s, 18H), 1.24 (s, 6H). **^{13}C NMR (101 MHz, CDCl$_3$)**: δ 167.73, 154.21, 145.95, 145.07, 144.60,133.60, 133.31, 132.35, 125.57, 124.74, 122.12, 121.33, 119.62, 116.41, 52.19, 34.26, 31.43, 26.99, 22.68. Compound **3** was subjected to the hydrolysis reaction without further purification. **3** (3.5 g, 4.00 mmol, 1 equiv.) was combined with sodium hydroxide (3.21 g, 80.18 mmol, 20 equiv.) in 900 mL of an THF/ethanol/water (1:1:1) mixture. The reaction was heated

to reflux for 12 h. After cooling to room temperature, the pH was adjusted to 2-3 by addition of dilute hydrochloric acid. The diacid precipitated as a yellow solid and was collected by vacuum filtration, washed thoroughly with water and hexane to afford thr target as a yellow powder. **Yield**. 2.1 g, 64%. **^{1}H NMR (500 MHz, DMSO)** δ 12.73 (s, 4H), 7.81 (d, J = 7.7 Hz, 4H), 7.43 (dd, J = 15.5, 7.9 Hz, 4H), 7.22 (d, J = 8.5 Hz, 4H), 6.89 (s, 2H), 6.83 (d, J = 8.5 Hz, 4H), 6.73 (d, J = 8.1 Hz, 2H), 1.26 (s, 18H), 1.18 (s, 6H). **^{13}C NMR (101 MHz, DMSO)** δ 168.06, 153.74, 145.99, 144.55, 143.93， 143.81, 134.30, 133.83, 132.44, 126.45, 125.71, 121.77, 120.67, 119.60, 115.65, 46.39, 34.36, 31.76, 27.41. **HRMS [M+H^{+}]**: Calculated: 817.34834 ($C_{51}H_{49}N_2O_8$); Found: 817.3468.

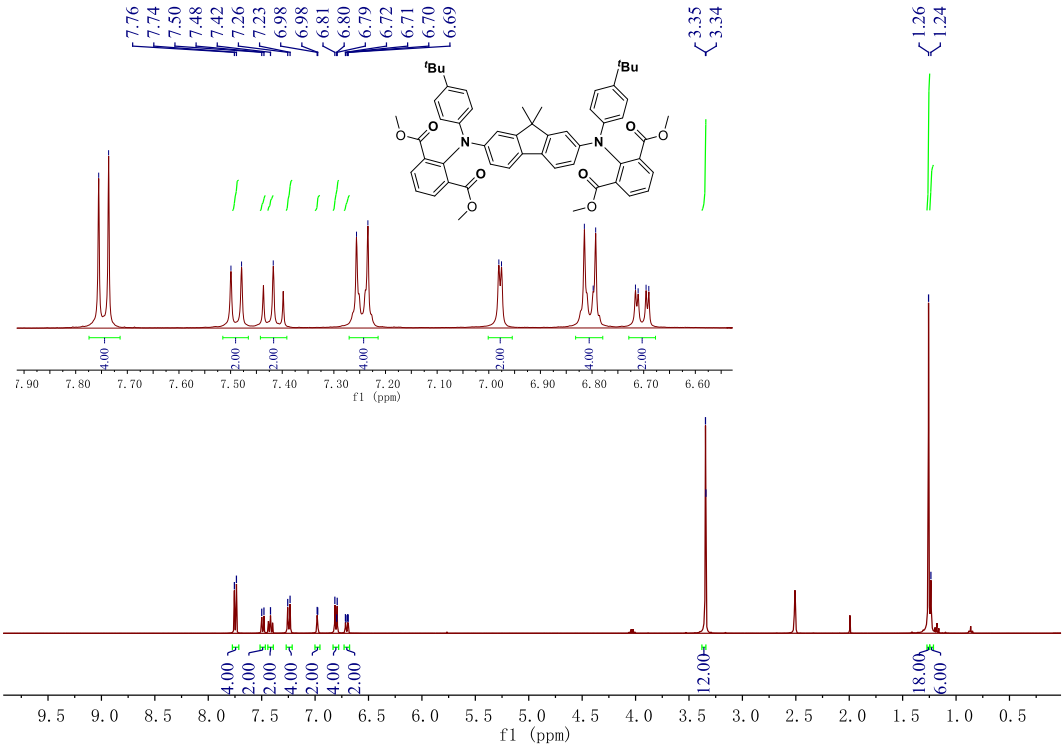

Figure **S5**. ^{1}H NMR spectrum of **3** in $CDCl_3$.

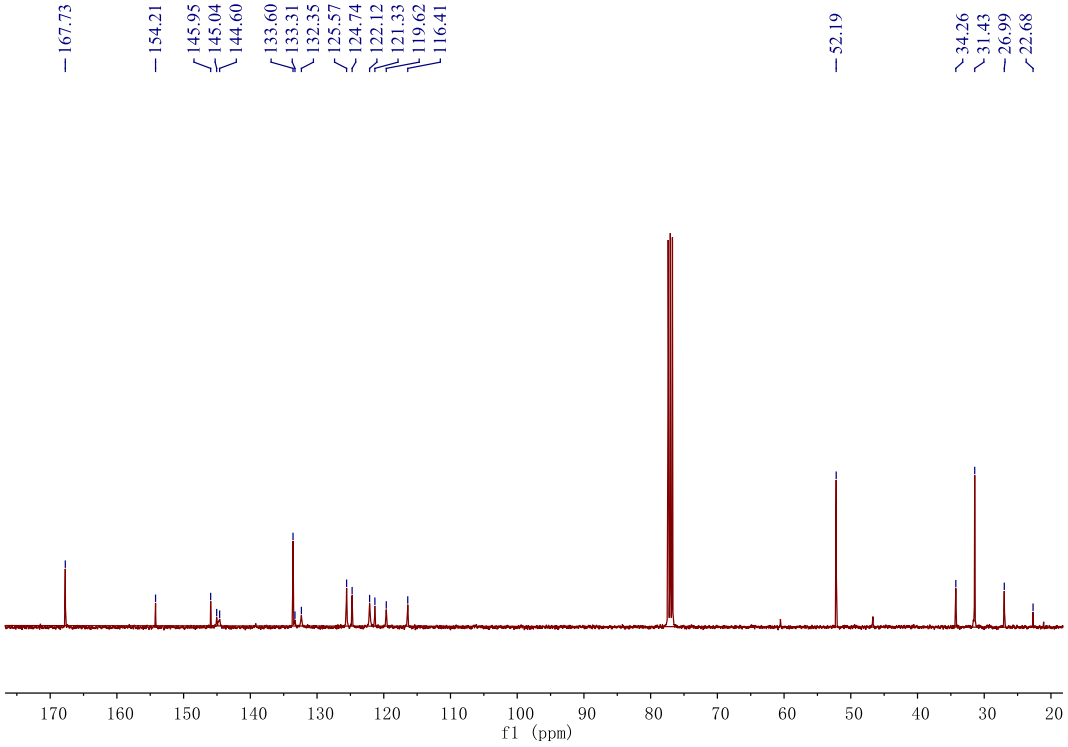

Figure **S6**. ^{13}C NMR spectrum of **3** in $CDCl_3$.

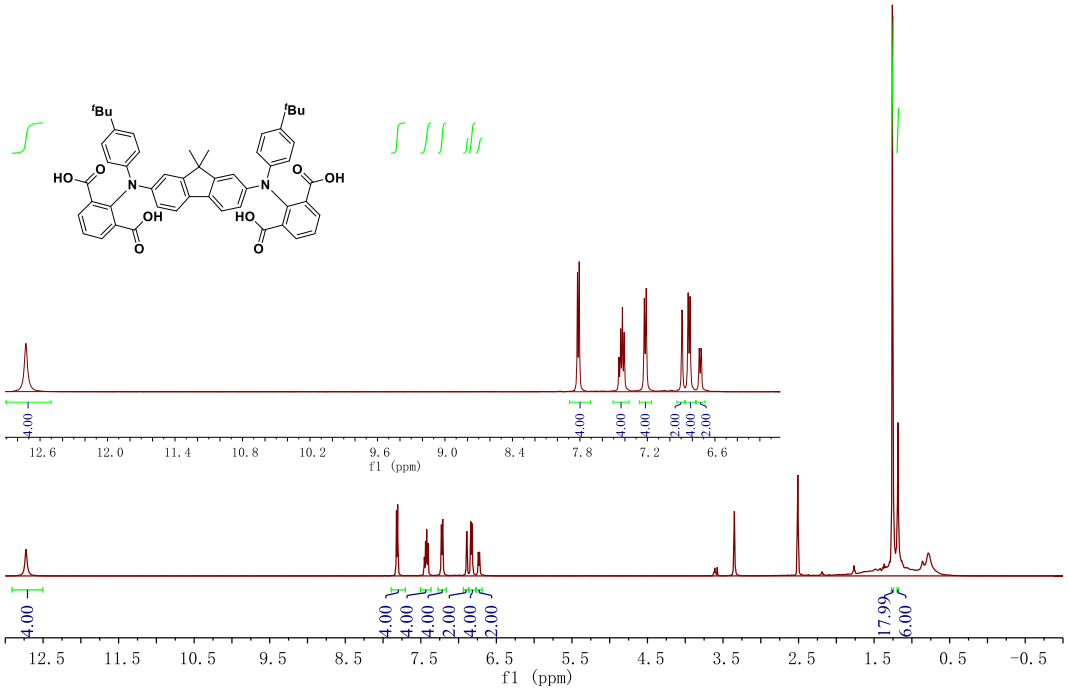

Figure **S7**. ^{1}H NMR spectrum of **4** in $CDCl_3$.

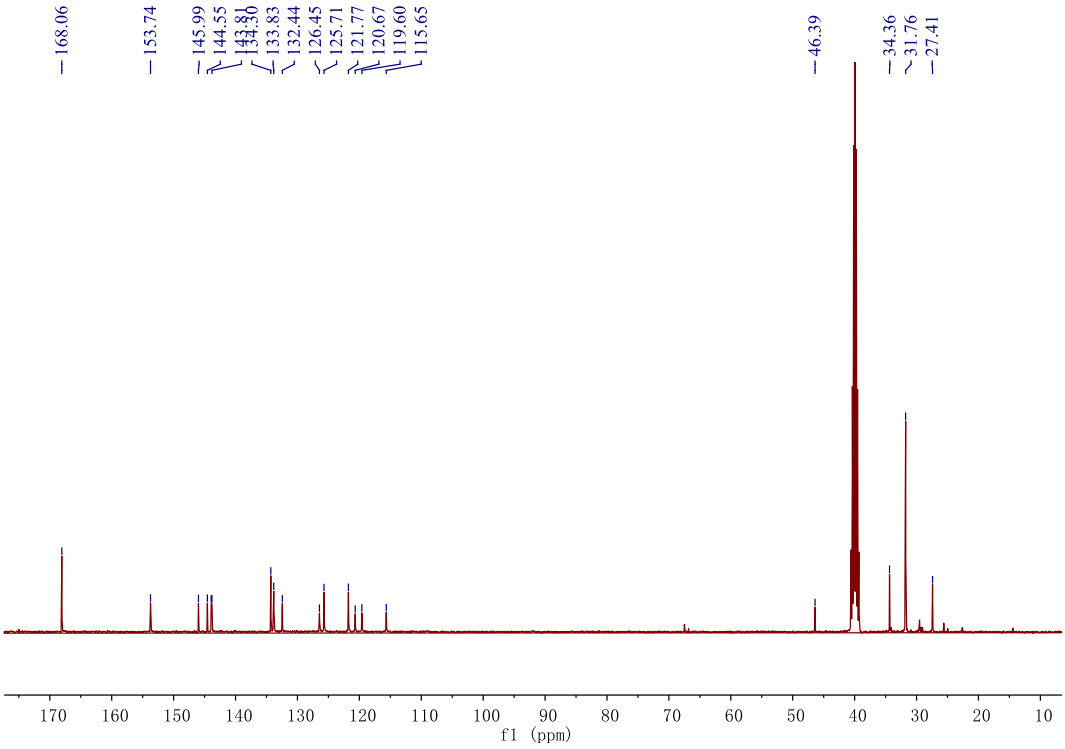

Figure **S8**. ^{13}C NMR spectrum of **4** in $CDCl_3$.

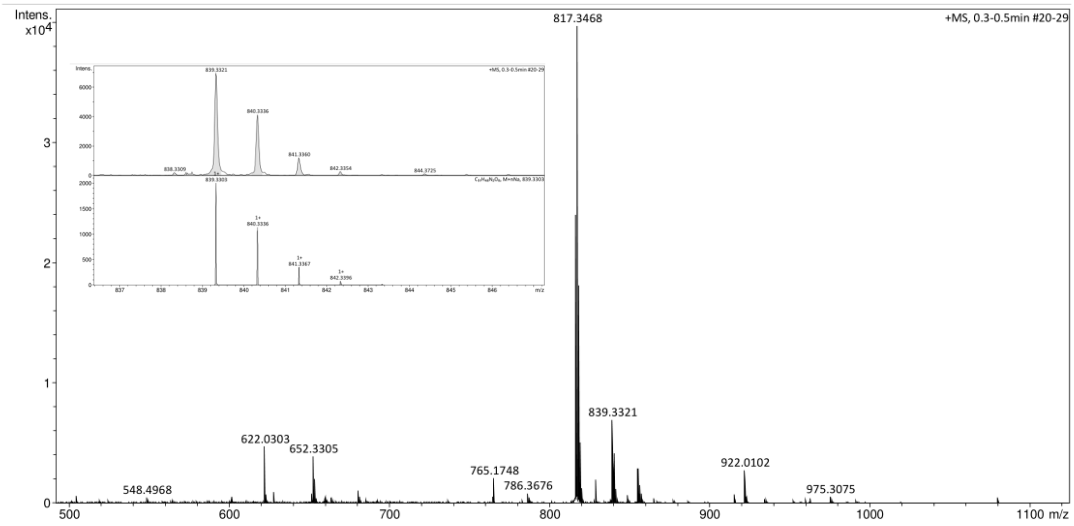

Figure **S9**. HRMS spectrum of **4**.

DDiKTa-F

4 (1.00 g, 1.22 mmol, 1 equiv.) was dispersed in 30 mL of DCM under a nitrogen atmosphere. To the reaction mixture were added sequentially thionyl chloride (0.45 mL, 6.12 mmol, 5.0 equiv.) and 2 drops of DMF. After 3 h under reflux, the reaction mixture was cooled to room temperature. Under a positive flow of nitrogen, $AlCl_3$ (1.63 g, 12.24 mmol, 10 equiv.) was added slowly. After heating at reflux for 12 h, the reaction mixture was cooled to room

temperature and the reaction was quenched by dropwise addition of water. The mixture was combined with dichloromethane (50 mL). The mixture was washed with a saturated NaCl aqueous solution (3 × 50 mL). The organic fractions were combined, and the solvent volume was concentrated under reduced pressure. The collected crude product was purified by silica gel column chromatography (EtOAc: DCM = 1:10, $\mathbf{R_f}$: 0.42) to afford the target compound as a yellow powder. **Yield**. 0.42 g, 46%. **Mp** > 400 °C. ^{1}H NMR (500 MHz, $CDCl_3$) δ 8.96 (s, 2H), 8.79 (dd, J = 12.7, 7.5 Hz, 4H), 8.55 (d, J = 2.3 Hz, 2H), 8.25 (s, 2H), 8.12 (s, 2H), 7.80 (s, 2H), 7.68 (t, J = 7.6 Hz, 2H), 1.59 (s, 6H), 1.50 (s, 18H). **^{13}C NMR (101 MHz, $CDCl_3$)** δ 181.32, 180.63, 159.61, 150.40, 140.35, 138.82, 137.93, 135.85, 135.08, 135.02, 132.24, 125.83, 125.40, 124.71, 124.21, 122.47, 122.28, 120.38, 115.64, 48.69, 35.07, 30.95, 27.01. **Anal. Calcd. For $C_{44}H_{40}BNO_4$**: C 82.23%, H 5.41%, N 3.76% **Found**: C 82.40%, H 5.52%, N 3.56%. **HRMS [M^+]**: Calculated: 745.3061 ($C_{51}H_{40}N_2O_4$); Found: 745.3050. 99.51% pure on HPLC analysis, retention time 10.490 minutes in 100% THF.

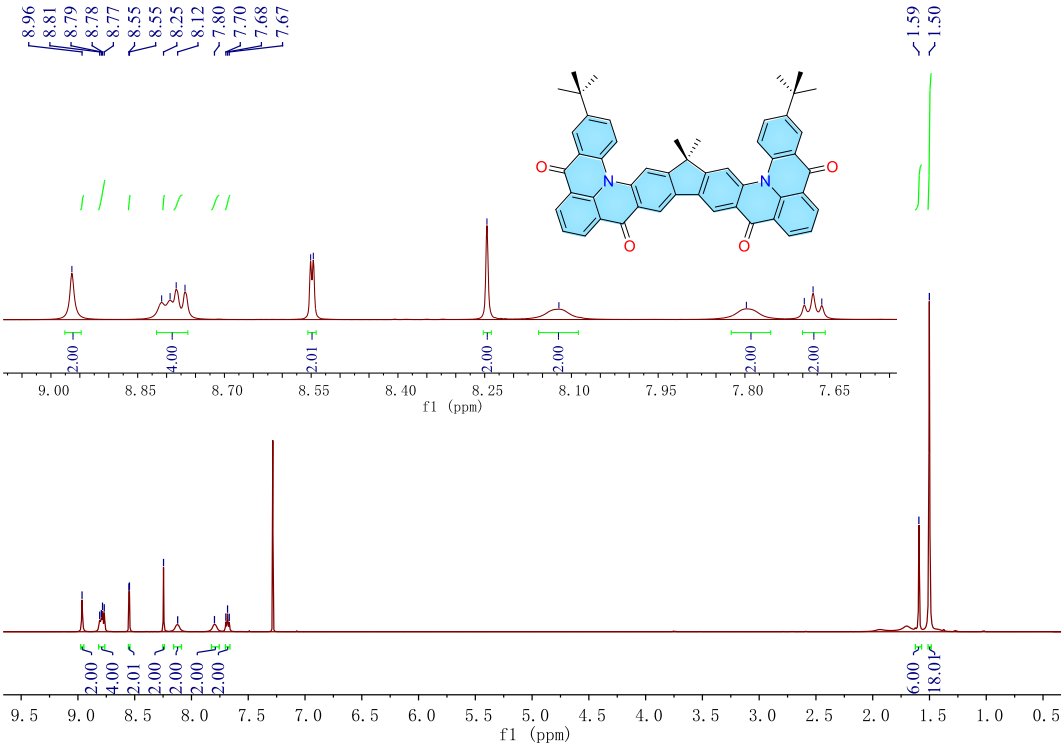

Figure **S10**. ^{1}H NMR spectrum of **DDiKTa-F** in $CDCl_3$.

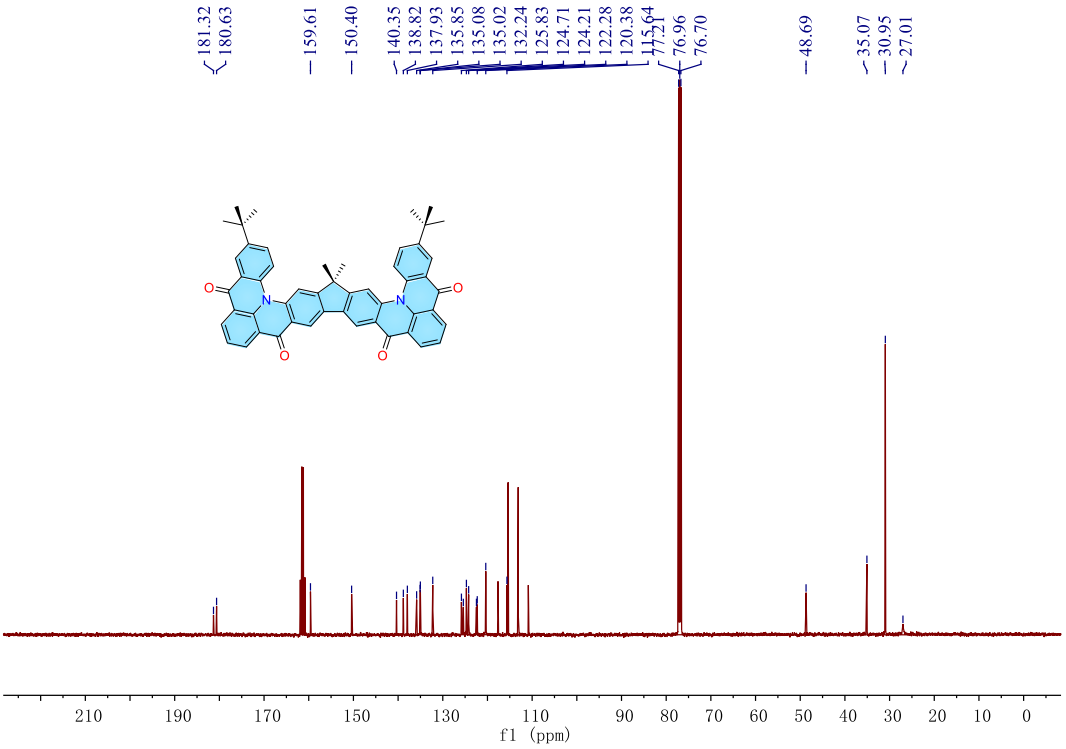

Figure **S11**. ^{13}C NMR spectrum of **DDiKTa-F** in $CDCl_3$.

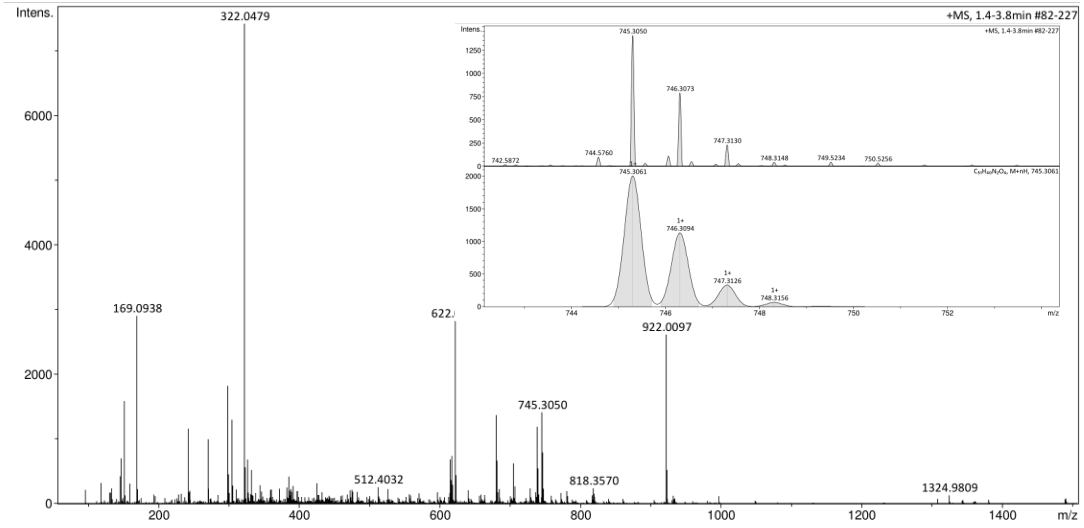

Figure **S12**. HRMS spectrum of **DDiKTa-F**.

NOTE: Please submit ca. 10 mg of sample

Sample reference number	WS-I196
Name of Compound	DDiKTa-F
Molecular formula	C51H40N2O4
Stability	
Hazards	
Other Remarks	

Analysis type:

Single ☐ **Duplicate** ☑ **Triplicate** ☐

Analysis Result:

Element	Expected %	Found (1)	Found (2)	Found (3)
Carbon	82.23	83.03	81.77	
Hydrogen	5.41	5.58	5.46	
Nitrogen	3.76	3.58	3.53	
Oxygen				

Authorising Signature:

Date completed	15.12.21
Signature	J Pl

Figure **S13**. Elemental analysis spectrum of **DDiKTa-F**.

Sample Name : DDIKTA-F
Sample ID : 001
Method Filename : 100% THF 20 mins 280nm.lcm
Batch Filename : DDIKTA-F.lcb
Vial # : 2-39
Injection Volume : 10 uL
Date Acquired : 08/10/2021 18:19:28
Date Processed : 08/10/2021 18:39:29

Sample Type : Unknown
Acquired by : System Administrator
Processed by : System Administrator

<Chromatogram>

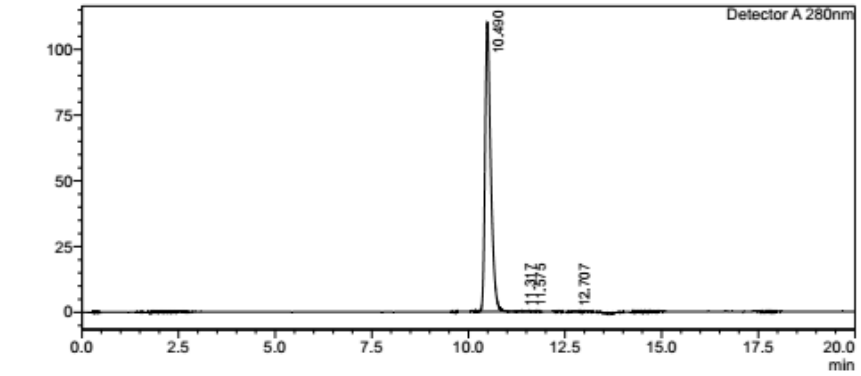

<Peak Table>

Detector A 280nm

Peak#	Ret. Time	Area	Height	Area%	Area/Height	Width at 5% Height
1	10.490	1133992	109819	99.506	10.326	0.366
2	11.317	2652	285	0.233	9.317	--
3	11.575	1104	98	0.097	11.293	--
4	12.707	1873	200	0.164	9.349	0.266
Total		1139620	110401	100.000		

Figure **S14**. HPLC spectrum of **DDiKTa-F**.

Computations

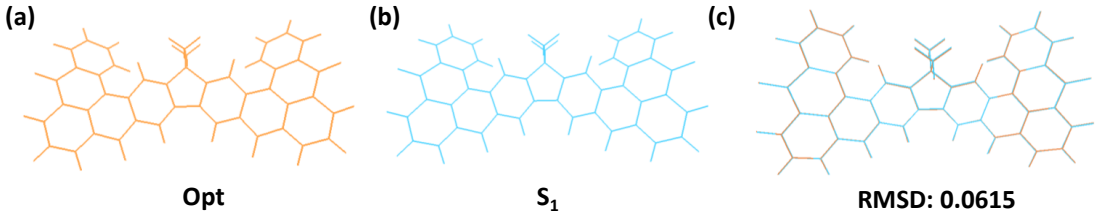

Figure **S15**. Optimized structures of the (a) ground state (S_0) and (b) excited singlet state (S_1); (c) the geometric difference between the S_0 and S_1 states. The root mean square deviation (RMSD) value between the two configurations is 0.0615.

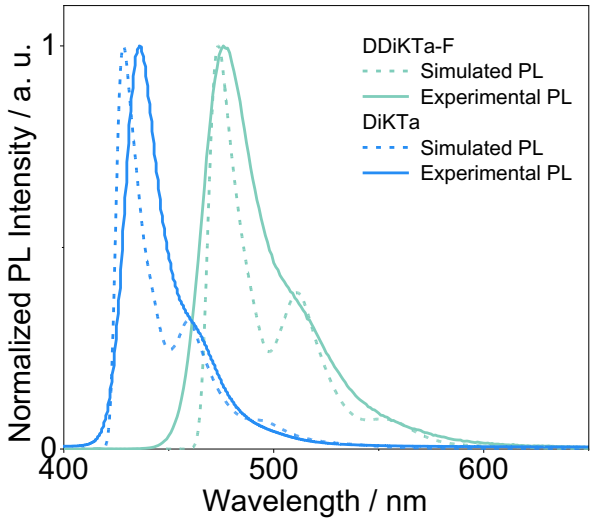

Figure **S16**. Emission spectra simulated by Franck-Condon analysis for the S_1-S_0 transition of **DDiKTa-F** and **DiKTa** under vacuum, and the experimental steady-state PL spectra of **DDiKa-F** in toluene and **DiKTa** in hexane.

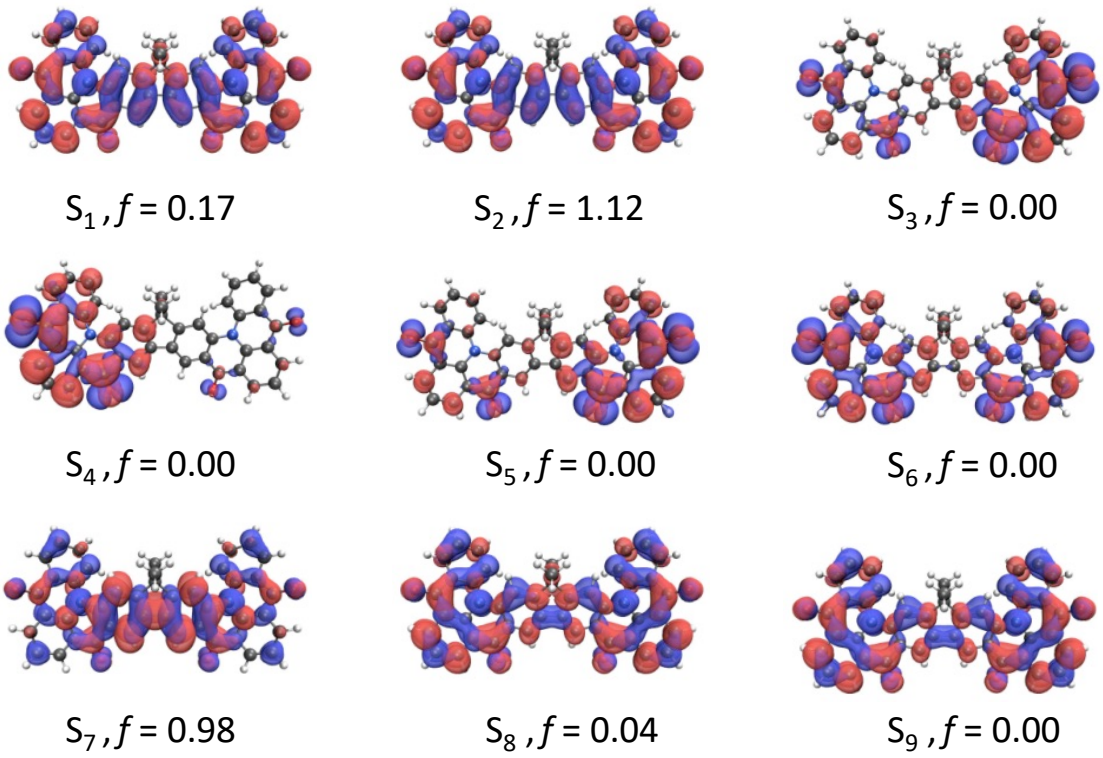

Figure **S17**. The natural transition orbitals (NTOs) for **DDiKTa-F** based on the optimized S_0 geometry.

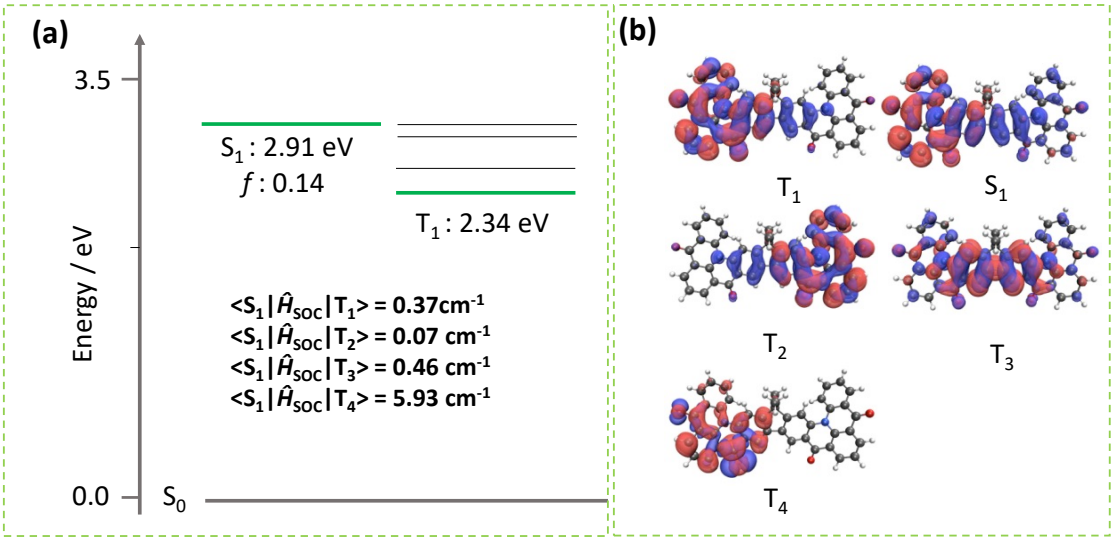

Figure **S18**. (a) Spin-orbit coupling matrix element (SOCME) for **DDiKTa-F** based on the optimized T_1 geometry. (b) the natural transition orbitals (NTOs) for the related excited states.

Optoelectronic Characterization

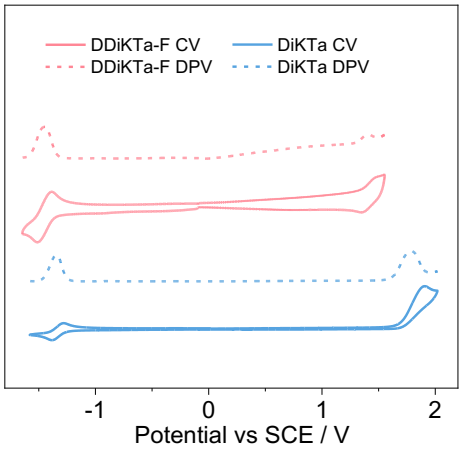

Figure **S19**. Cyclic voltammogram (CV) and differential pulse voltammetry (DPV) in degassed DCM with 0.1 M [^{n}Bu$_4$N]PF$_6$ as the supporting electrolyte and Fc/Fc$^+$ as the internal reference versus SCE (0.46 V vs. DCM).[16]

Table **S1.** Electrochemical data

Material	E_{ox} /V[a]	E_{red} /V[a]	ΔE /V[b]	E_{HOMO} / eV[c]	E_{LUMO} /eV[c]
DDiKTa-F	1.34	-1.48	2.82	-5.68	-2.86
DiKTa	1.78	-1.35	3.03	-6.12	-2.99

[a] E_{ox} and E_{red} are the peak of anodic and cathodic potentials from DPV versus SCE. In degassed DMF with 0.1 M [^{n}Bu$_4$N]PF$_6$ as the supporting electrolyte and Fc/Fc$^+$ as the internal reference (0.46 V vs. SCE).[16] [b] $\Delta E = E_{ox}$-E_{red}. [c] $E_{HOMO/LUMO}$ = -(E_{ox} / E_{red} vs. Fc/Fc$^+$ + 4.8) eV.[17]

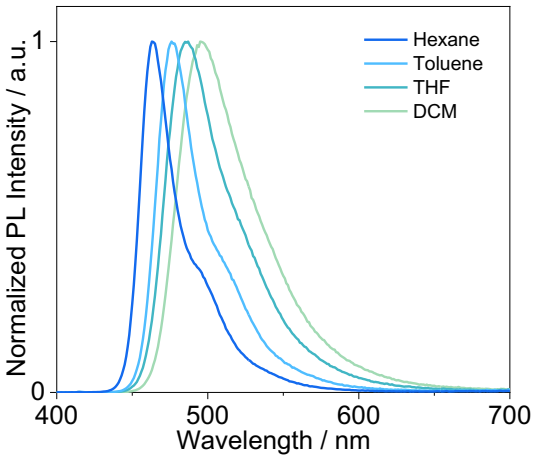

Figure **S20**. Solvatochromism PL study for **DDiKTa-F**. λ_{exc} = 340 nm.

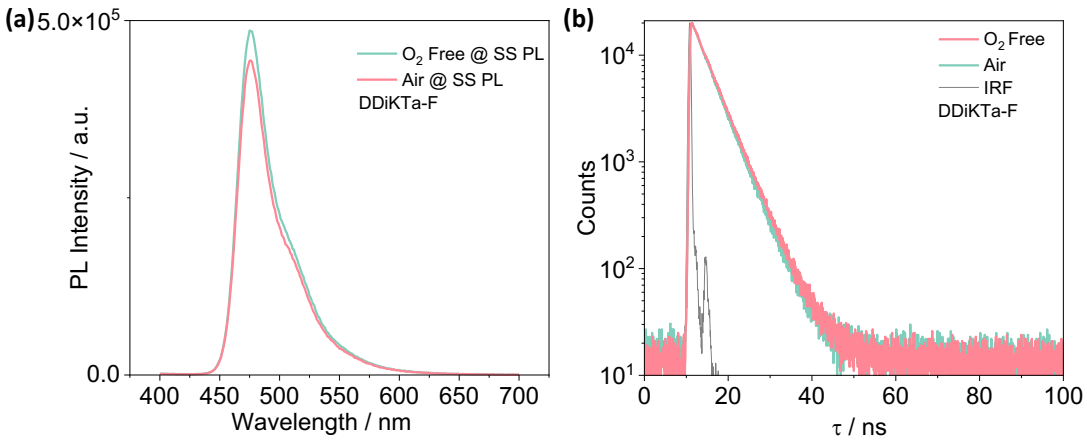

Figure **S21**. Comparison of the intensity of the PL spectra in both aerated and degassed toluene solutions (λ_{exc} = 340 nm); (b) Time-resolved PL decays (λ_{exc} = 375 nm) in toluene solution of **DDiKTa-F**

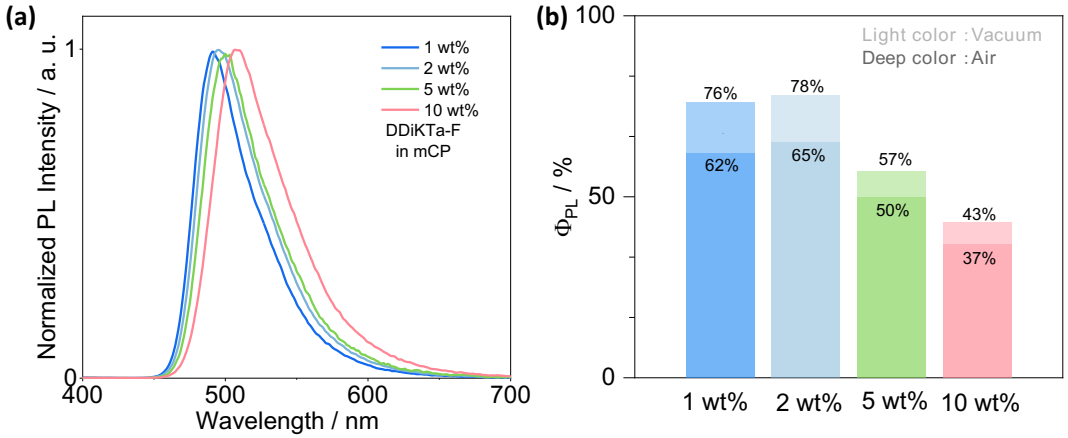

Figure **S22**. (a) Concentration-dependent PL of **DDiKTa-F** in mCP doped films under air; (b) Concentration-dependent Φ_{PL} of **DDiKTa-F** in mCP doped films under air and nitrogen, λ_{exc}=340 nm.

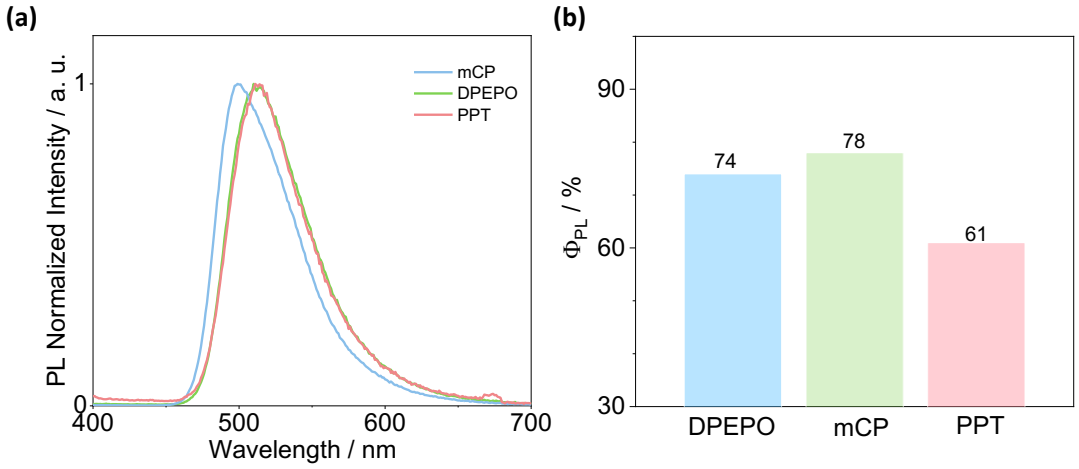

Figure **S23**. (a) SSPL and (b) Φ_{PL} of **DDiKTa-F** under nitrogen as 2 wt% doped film in different hosts, λ_{exc}=340 nm.

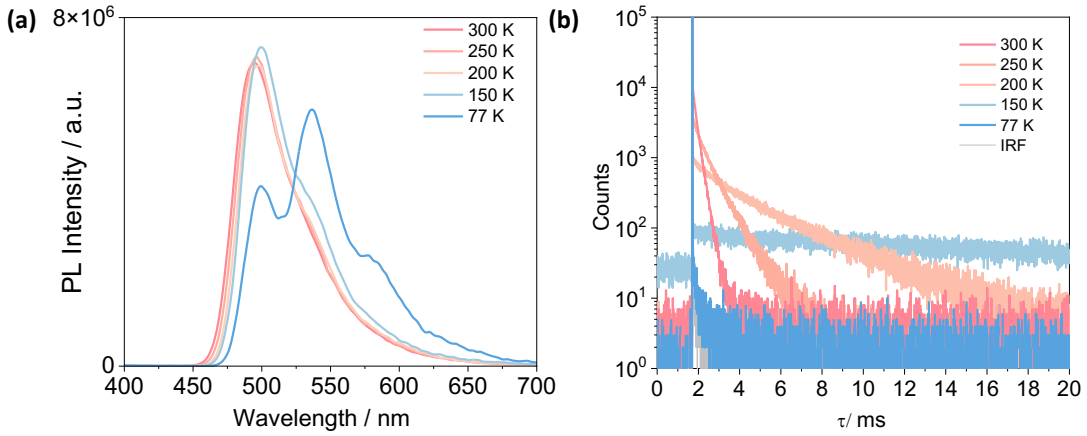

Figure **S24**. Temperature-dependent (a) steady-state PL spectra, λ_{exc} = 340 nm; (b) temperature-dependent transient decays of 2 wt% doped films of **DDiKTa-F** in mCP, λ_{exc} = 379 nm.

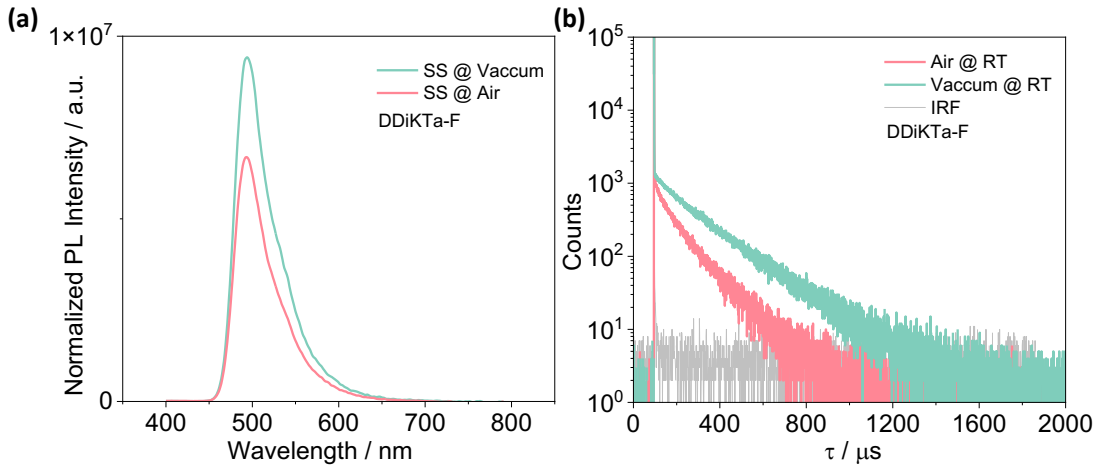

Figure **S25**. Aerated and degassed comparison of (a) SSPL, λ_{exc} = 340 nm; (b) TRPL decay of 2 wt% doped film of **DDiKTa-F** in mCP. λ_{exc} = 379 nm.

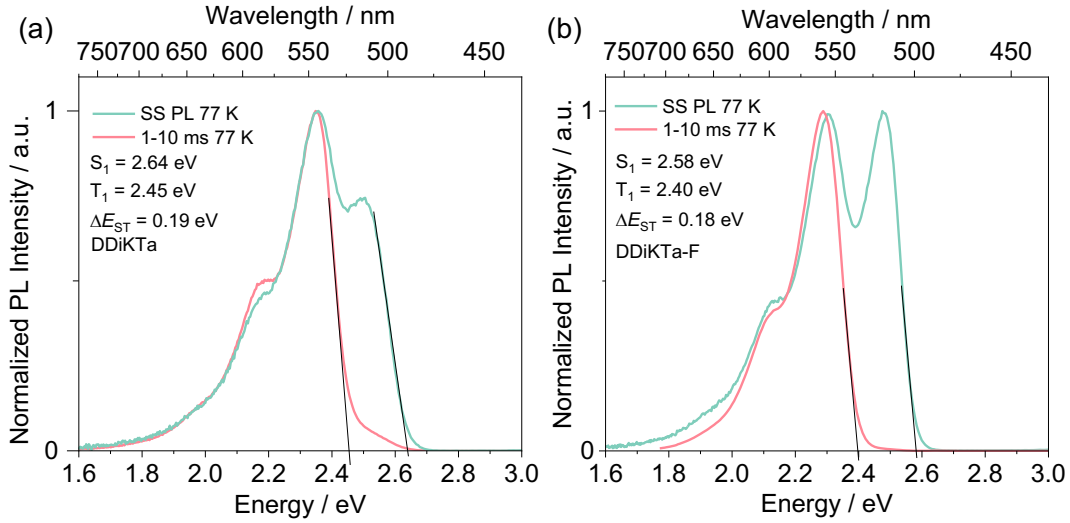

Figure **S26**. SS PL and delayed emission spectra of (a) **DDiKTa** and (b) **DDiKTa-F** measured in 2 wt% doped film in mCP at 77 K, λ_{exc} = 340 nm.

For a TADF system, the main exciton loss channels are either singlet or triplet nonradiative transition processes. Considering the PLQY of 78% for **DDiKTa-F**, the singlet nonradiative transition process (k_{nr}^{S}) can be ignored, therefore the exciton loss can be attributed to the triplet nonradiative transition process (k_{nr}^{T}). The kinetics parameters were calculated according to the following equations and summarized in Table **S2**.[21,22]

$$\Phi_{PL} = \Phi_p + \Phi_d \quad (1)$$

$$k_P = \frac{1}{\tau_p} \quad (2)$$

$$k_d = \frac{1}{\tau_d} \quad (3)$$

$$k_r^S = k_p \Phi_p \quad (4)$$

$$k_{ISC} = k_p(1 - \Phi_p) \quad (5)$$

$$k_{RISC} = \frac{k_p k_d}{k_{ISC}} \frac{\Phi_d}{\Phi_p} \quad (6)$$

$$k_{nr}^T = k_d - \Phi_p k_{RISC} \quad (7)$$

Where the Φ_p and Φ_d are the prompt fluorescence and delayed fluorescence quantum efficiencies; k_p is the rate constant of prompt fluorescence; k_d is the rate constant of delayed fluorescence; k_r^S is the radiative decay rate constant of S_1; k_{nr}^T is the non-radiative decay rate constant of T_1; k_{ISC} is the intersystem crossing rate constant; k_{RISC} is the reverse intersystem crossing rate constant.

Table **S2.** Summary of kinetics parameters of 2 wt% doped films in mCP.

Compounds	Φ_P /%	Φ_d /%	k_p / 10^8 s^{-1}	k_d / 10^3 s^{-1}	k_r^S /10^7 s^{-1}	k_{nr}^T /10^3 s^{-1}	k_{ISC} /10^8 s^{-1}	k_{RISC} /10^4 s^{-1}
DDiKTa-F	18	60	1.79	5.32	3.21	1.43	1.46	2.16
DDiKTa	21	47	1.69	6.25	3.56	2.53	1.34	1.77
DiKTa[23]	7	39	2.08	0.41	1.44	2.40	1.94	2.52

Devices

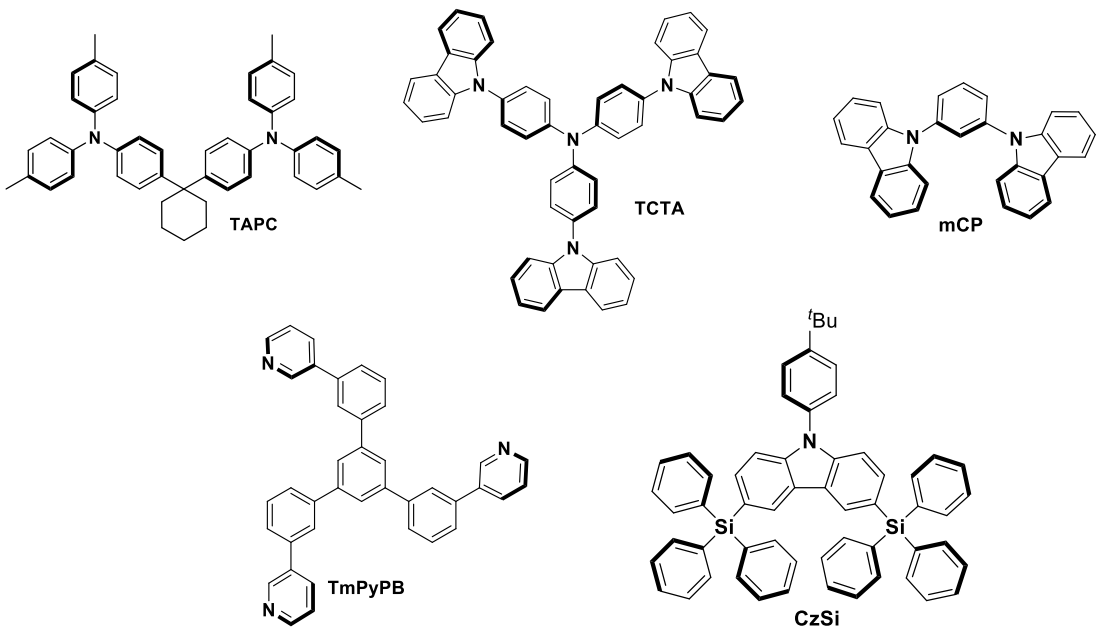

Figure **S27**. Molecular structures of materials used in the devices.

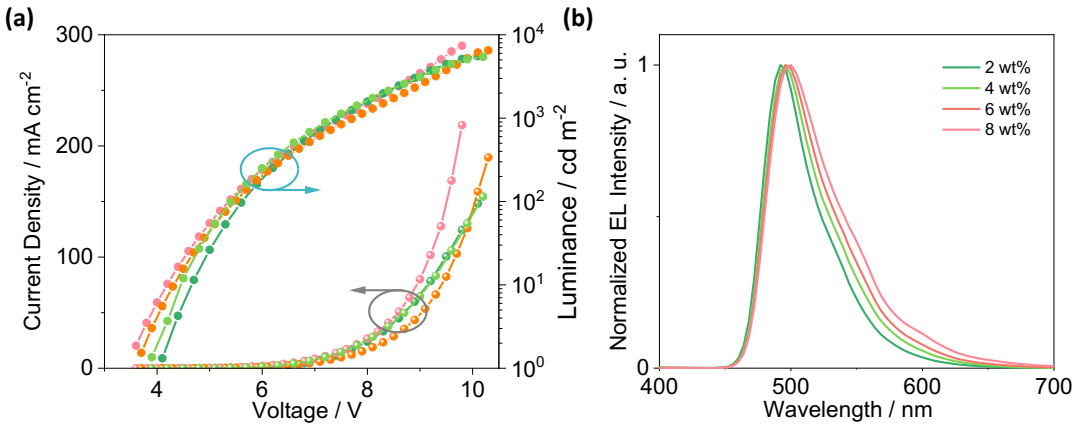

Figure **S28**. (a) *J*–*V*–*L* characteristics and (b) electroluminescent spectra for devices for different doped concentration.

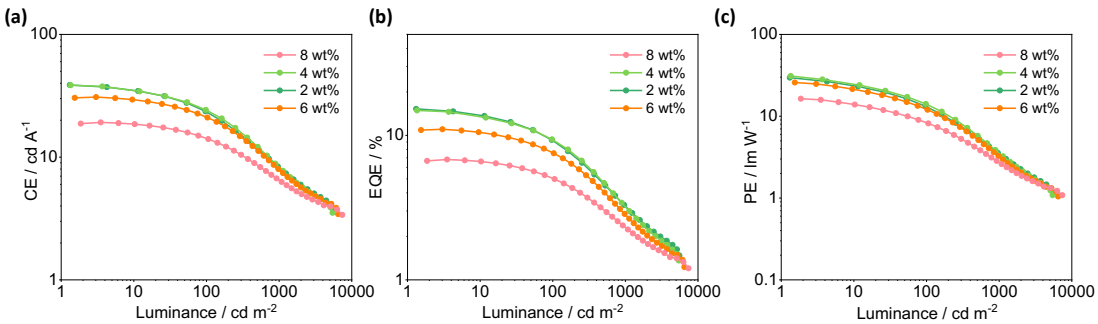

Figure **S29**. (a) CE, (b) EQE and (c) PE versus luminance characteristics.

Table **S3**. Electroluminescence data.

Device	V_{on}[a] / V	λ_{EL} / nm	FWHM[b] / nm	CIE (x,y)	L_{max}[c] /cd m^{-2}	$EQE_{max/100/1000}$[d] / %
DDiKTa-F	4.1	493	46	0.16, 0.50	5551	15.3/9.9/3.3
DDiKTa[24]	3.7	500	59	0.18, 0.53	504	19.0/8.07
DiKTa[25]	3.0	465	39	0.14, 0.18	10385	14.7/8.3/3.3

[a] Turn-on voltage at the luminance of 1 cd m^{-2}. [b] Full width at half-maximum of the EL spectrum. [c] Maximum luminance. [d] Maximum external quantum efficiency/EQE at 100 cd m^{-2}/EQE at 1000 cd m^{-2}.

References

1 M. J. Frisch, G. W. Trucks, H. B. Schlegel, G. E. Scuseria, M. A. Robb, J. R. Cheeseman, G. Scalmani, V. Barone, G. A. Petersson, H. Nakatsuji, X. Li, M. Caricato, A. V. Marenich, J. Bloino, B. G. Janesko, R. Gomperts, B. Mennucci, H. P. Hratchian, J. V. Ortiz, A. F. Izmaylov, J. L. Sonnenberg, Williams, F. Ding, F. Lipparini, F. Egidi, J. Goings, B. Peng, A. Petrone, T. Henderson, D. Ranasinghe, V. G. Zakrzewski, J. Gao, N. Rega, G. Zheng, W. Liang, M. Hada, M. Ehara, K. Toyota, R. Fukuda, J. Hasegawa, M. Ishida, T. Nakajima, Y. Honda, O. Kitao, H. Nakai, T. Vreven, K. Throssell, J. A. Montgomery Jr., J. E. Peralta, F. Ogliaro, M. J. Bearpark, J. J. Heyd, E. N. Brothers, K. N. Kudin, V. N. Staroverov, T. A. Keith, R. Kobayashi, J. Normand, K. Raghavachari, A. P. Rendell, J. C. Burant, S. S. Iyengar, J. Tomasi, M. Cossi, J. M. Millam, M. Klene, C. Adamo, R. Cammi, J. W. Ochterski, R. L. Martin, K. Morokuma, O. Farkas, J. B. Foresman, D. J. Fox, Wallingford, CT 2016

2 N. O. C. Winter and C. Hättig, *J. Chem. Phys.*, 2011, **134**, 184101.

3 a. d. o. U. o. K. a. F. TURBOMOLE V7.4 2017 and -. Karlsruhe GmbH, TURBOMOLE GmbH, since S105 2007, 1989-2007.

4 S. Hirata and M. Head-Gordon, *Chem. Phys. Lett.*, 1999, **314**, 291–299.

5 T. H. Dunning Jr., *J. Chem. Phys.* , 1989, **90**, 1007–1023.

6 S. Grimme, *Chem. Phys. Lett.*, 1996, **259**, 128–137.

7 X. Gao, S. Bai, D. Fazzi, T. Niehaus, M. Barbatti and W. Thiel, *J. Chem. Theory Comput.*, 2017, **13**, 515–524.

8 *Nielsen, A.B. and Holder, A.J. (2009) Gauss View 5.0, User's Reference. GAUSSIAN Inc., .*

9 N. M. O'Boyle, A. L. Tenderholt and K. M. Langner, *J Comput Chem*, 2008, **29**, 839–845.

10 J. D. Hunter, *Computing in Science & Engineering*, 2007, **9**, 90–95.

11 M. M. McKerns, L. Strand, T. Sullivan, A. Fang, M. A. G. Aivazis and S. M. J. van der Walt, 2011.

12 Koichi Momma and Fujio Izumi, *J. Appl. Crystallogr.*, 2008, **41**, 653–658.

13 W. Humphrey, A. Dalke and K. Schulten, *J. Mol. Graph.*, 1996, **14**, 33–38.

14 F. Santoro, A. Lami, R. Improta, J. Bloino and V. Barone, *J. Chem. Phys.*, 2008, **128**, 224311.

15 J. Tirado-Rives and W. L. Jorgensen, *J. Chem. Theory Comput.*, 2008, **4**, 297–306.

16 N. G. Connelly and W. E. Geiger, *Chem. Rev.*, 1996, **96**, 877–910.

17 C. M. Cardona, W. Li, A. E. Kaifer, D. Stockdale and G. C. Bazan, *Adv. Mater.*, 2011, **23**, 2367–2371.

18 G. A. Crosby and J. N. Demas, *J. Phys. Chem.*, 1971, **75**, 991–1024.

19 W. H. Melhuish, *J. Phys. Chem.*, 1961, **65**, 229–235.

20 A. M. Johnson, C. A. Wiley, M. C. Young, X. Zhang, Y. Lyon, R. R. Julian and R. J. Hooley, *Angew. Chem., Int. Ed.*, 2015, **54**, 5641–5645.

21 K. Masui, H. Nakanotani and C. Adachi, *Org. Electron.*, 2013, **14**, 2721–2726.

22 Y. Tsuchiya, S. Diesing, F. Bencheikh, Y. Wada, P. L. dos Santos, H. Kaji, E. Zysman-Colman, I. D. W. Samuel and C. Adachi, *J. Phys. Chem. A*, 2021, **125**, 8074–8089.

23 S. Wu, L. Zhang, J. Wang, A. Kumar Gupta, I. D. W. Samuel and E. Zysman-Colman, *Angew. Chemie Int. Ed.*, 2023, **62**, e202305182.

24 D. Sun, S. M. Suresh, D. Hall, M. Zhang, C. Si, D. B. Cordes, A. M. Z. Slawin, Y. Olivier, X. Zhang and E. Zysman-Colman, *Mater. Chem. Front.*, 2020, **4**, 2018–2022.

25 D. Hall, S. M. Suresh, P. L. dos Santos, E. Duda, S. Bagnich, A. Pershin, P. Rajamalli, D. B. Cordes, A. M. Z. Slawin, D. Beljonne, A. Köhler, I. D. W. Samuel, Y. Olivier and E. Zysman-Colman, *Adv. Opt. Mater.*, 2020, **8**, 1901627.